

Virus shapes and buckling transitions in spherical shells

Jack Lidmar

Department of Physics, Royal Institute of Technology, AlbaNova, SE-106 91 Stockholm, Sweden

Leonid Mirny

*Harvard-MIT Division of Health Science and Technology,
Massachusetts Institute of Technology, Cambridge, MA 02139, USA*

David R. Nelson

Lyman Laboratory of Physics, Harvard University, Cambridge, MA 02138, USA

(Dated: January 28, 2020)

We show that the icosahedral packings of protein capsomeres proposed by Caspar and Klug for spherical viruses become unstable to faceting for sufficiently large virus size, in analogy with the buckling instability of disclinations in two-dimensional crystals. Our model, based on the nonlinear physics of thin elastic shells, produces excellent one parameter fits in real space to the full three-dimensional shape of large spherical viruses. The faceted shape depends only on the dimensionless Foppl-von Kármán number $\gamma = YR^2/\kappa$, where Y is the two-dimensional Young's modulus of the protein shell, κ is its bending rigidity and R is the mean virus radius. The shape can be parameterized more quantitatively in terms of a spherical harmonic expansion. We also investigate elastic shell theory for extremely large γ , $10^3 < \gamma < 10^8$, and find results applicable to icosahedral shapes of large vesicles studied with freeze fracture and electron microscopy.

I. INTRODUCTION

Understanding virus structures is a rich and challenging problem [1], with a wealth of new information now becoming available. Although traditional X-ray crystallography still allows the most detailed analysis [2], three-dimensional reconstructions of icosahedral viruses from cryo-electron micrographs are now becoming routine [3]. Electron microscope images of many identical viruses in a variety of orientations are used to reconstruct a three-dimensional image on a computer, similar to CT (computed tomography) scans in medical imaging. There are now, in addition, beautiful single molecule experiments which measure the work needed to load a virus (bacteriophage $\phi29$) with its DNA package [4]. The aim of this paper is to explore the elastic parameters and physical ideas which determine the shapes of viruses with an icosahedral symmetry, using the theory of thin elastic shells [5].

The analysis of approximately spherical viruses dates back to pioneering work by Crick and Watson in 1956 [6], who argued that the small size of the viral genome requires identical structural units packed together with an icosahedral symmetry. These principles were put on a firm basis by Caspar and Klug in 1962 [7], who showed how the proteins in a viral shell (the “capsid”) could be viewed as icosadeltahedral triangulations of the sphere by a set of pentavalent and hexavalent morphological units (“capsomeres”). The viral shells (there can also be an outer envelope composed of additional proteins and membrane elements from the host cell) are characterized by a pair of integers (h, k) such that the number of morphological units is $N = 10(h^2 + hk + k^2) + 2$. To get from one pentavalent capsomer to another, one moves h capsomeres along a row of near-neighbor bonds on the

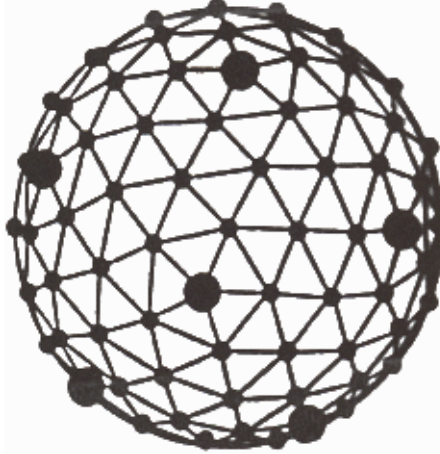


FIG. 1: A right-handed (3,1) triangulated net (icosadeltahedron) used to describe virus structure. The (1,3) structure is left-handed.

sphere, turns 120 degrees and moves another k steps. Euler's theorem relating the number of vertices, edges and faces of a spherical triangulation insures that the number of capsomeres in five-fold environments is exactly 12 [8]. A simple icosahedron of 12 morphological units corresponds to (1,0) while soccer balls and C_{60} fullerene molecules are (1,1) structures with $N = 32$ polygons. A (3,1) icosadeltahedron $N = 132$ is shown in Fig. 1. The polyoma virus (SV40) is a (2,1) structure with 72 capsomeres, while the much larger adenovirus and herpes simplex virus are (5,0) and (4,0) structures with 252 and 162 morphological units, respectively. Structures like that in Fig. 1 with h and k nonzero and $h \neq k$ are chiral.

Note that the relatively small polyoma virus (diameter

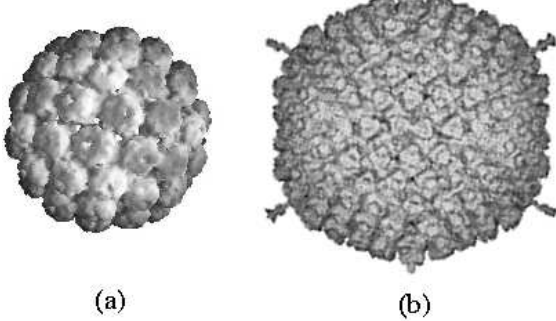


FIG. 2: The polyoma virus (a) is approximately spherical, while the larger adenovirus (b) is more faceted (not to scale). Images from Ref. [9].

440 Angstroms) is round (see Fig. 2a), while the much larger herpes simplex virus (diameter 1450 Angstroms) has a more angular or faceted shape [9] (see Fig. 2b). Faceting of large viruses is in fact a common phenomenon; the protein subunits of different viruses, moreover, are very similar (see below). If these protein assemblies are characterized by elastic constants and a bending rigidity [5], we can ask how deviations from a spherical shape develop with increasing virus radius, which scales roughly as the square root of the number of morphological units.

In support of the idea that viruses with different overall capsid size are composed of nearly identical monomers, we note that most viral coat and capsid proteins have about the same size, molecular weight, amino acid composition and, most importantly, the same folded structure in three dimensions [10]. It is known, moreover, that protein structure determines the mechanical properties of proteins [11, 12]. Hence, the similarity of the protein structure of the coat/capsid proteins suggests similar mechanical properties. In addition, the presence of the same fold of capsid proteins in unrelated viruses (bacterial phages, plant viruses, insect viruses and animal viruses) indicate that the fold and its mechanical properties are conserved in evolution and could be essential for proper virus assembly.

In this paper, we argue that the faceting of large viruses is caused by a buckling transition associated with the 12 isolated points of 5-fold symmetry. These singularities can be viewed as disclinations in an otherwise 6-coordinated medium. It is well known that the large strains associated with an isolated disclination in a *flat* disk spanned by a triangular lattice leads to buckling into a conical shape for [13, 14]

$$YR^2/\kappa \geq 154, \quad (1)$$

where Y is the two-dimensional Young's modulus, κ is the

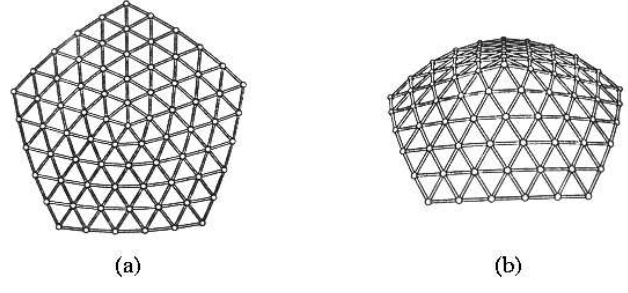


FIG. 3: The fivefold disclination in a triangular lattice. In viruses, the points would correspond to capsomeres, while in lecithin vesicles they correspond to lipid molecules. The highly strained flat space configuration is shown in (a). The buckled form which arises for $\gamma \geq 154$ is shown in (b).

bending rigidity and R is the disk radius. The energy of a single 5-fold disclination with “charge” $s = 2\pi/6$ centered in a flat array of proteins of size R is approximately

$$E_5 \approx \frac{1}{32\pi} s^2 Y R^2. \quad (2)$$

However, above a critical buckling radius $R_b \approx \sqrt{154\kappa/Y}$, is there a conical deformation (see Fig. 3) such that the disclination energy now only grows logarithmically with R

$$E_5 \approx (\pi/3)\kappa \ln(R/R_b) + \frac{1}{32\pi} s^2 Y R_b^2. \quad (3)$$

One might expect a similar phenomenon for 12 disclinations confined to a surface with a *spherical* topology. Indeed, the elastic energy for 12 disclinations on an undeformed sphere of radius R has a form similar to Eq. (2), namely [15]

$$E \approx 0.604(s^2 Y R^2 / 4\pi), \quad (4)$$

where the sphere radius R now plays the role of the system size. Although it seems highly likely that these 12 disclinations can lower their energy by buckling for large R , the nonlinear nature of the underlying elastic theory [5] leads to complex interactions between the resulting conical deformations. A boundary layer analysis of the von Kármán equations for bent plates predicts anomalous scaling for the mean curvature in the vicinity of the ridges connecting conical singularities [16, 17]. Interesting scaling behavior also arises in the vicinity of the apexes of the cones themselves [18]. Another interesting physical realization of the buckling problem lies in the faceting of lecithin vesicles at temperatures sufficiently low so that the lipid constituents have crystallized [19, 20].

In this paper, we study the ground states of crystalline particle arrays with 12 disclinations in a spherical geometry. We find that there are indeed striking manifestations of the buckling transition even in the curved geometry of

viral capsids or crystalline vesicles. The nonlinear Foppl-von Kármán equations for thin shells with elasticity and a bending energy are solved using a floating mesh discretization developed and studied extensively in the context of “tethered surface” models of polymerized membranes [21]. By taking the nodes of the mesh to coincide with the capsomers, even small viruses can be handled in this way, although any buckling transition will surely be smeared out unless R_b/a is large, where a is the spacing between these morphological units. Ideas from continuum elastic theory will, of course, be most applicable for vesicles composed of many lipids and for large viruses — Viruses with as many as 1692 morphological units have been reported [22].

There may be inherent limitations on the size of viral capsids that follow from the elastic properties of thin shells. Because larger viruses can accommodate more genetic material, large sizes could confer an evolutionary advantage. If, however, large viruses buckle away from a spherical shape, the resistance of the capsid to mechanical deformation can degrade. As we shall see, a theory of buckled crystalline order on spheres also allows estimates of important macroscopic elastic parameters of the capsid shell from structural data on the shape anisotropy. Estimates of quantities such as the bending rigidity and Young’s modulus of an empty viral shell might allow an understanding of deformations due to loading with DNA or RNA [4]. Although some aspects of virus structure may be accounted for by the physics of shell theory, we should emphasize that other features could be driven by the need for cell recognition, avoidance of immune response, etc.

A summary of our investigations of buckling transitions in a spherical geometry (discussed in detail in Sec. II) is shown in Fig. 4. As illustrated in Fig. 4 (See also Fig. 5) icosahedral shells do indeed become aspherical as the “Foppl-von Kármán number” $\gamma = YR^2/\kappa$ increases from values of order unity to $YR^2/\kappa \gg 1$. The mean square “asphericity” (deviation from a perfect spherical shape) departs significantly from zero when YR^2/κ exceeds 154, the location of the buckling transition in flat space [13]. Fits of buckled viruses or crystalline vesicles to this universal curve would allow an experimental determination of the ratio Y/κ . More quantitative information on the buckled shape can be obtained by expanding the radius $R(\theta, \phi)$ in spherical harmonics,

$$R(\theta, \phi) = \sum_{\ell=0}^{\infty} \sum_{m=-\ell}^{\ell} Q_{\ell m} Y_{\ell m}(\theta, \phi), \quad (5)$$

and studying the rotationally invariant quadratic invariants allowed for viruses or vesicles with icosahedral symmetry, namely

$$\hat{Q}_{\ell} = \sqrt{\frac{1}{2\ell+1} \sum_{m=-\ell}^{\ell} |Q_{\ell m}|^2 / Q_{00}} \quad (6)$$

with $\ell = 0, 6, 10, 12, 16, 18, \dots$ [23]. Although *any* pa-

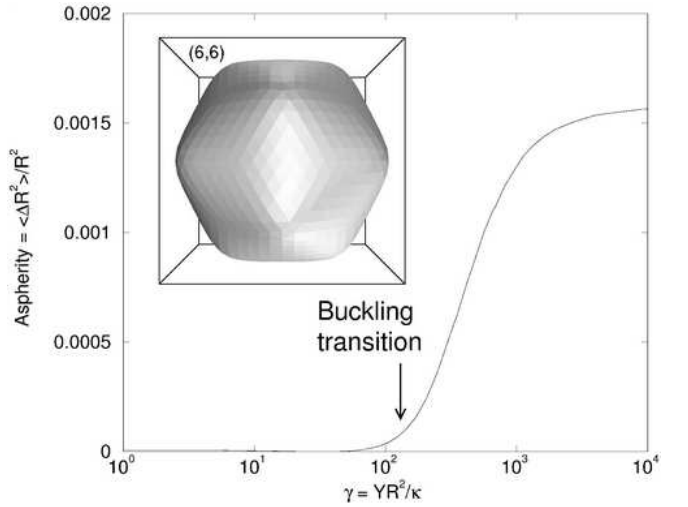


FIG. 4: Mean square asphericity as a function of YR^2/κ for many different icosahedral shells. The inset shows a (6,6) structure with Foppl-von Kármán number $\gamma = YR^2/\kappa \approx 400$. The arrow marks the location of the buckling transition in flat space.

rameter set of the form $\{\hat{Q}_6, \hat{Q}_{10}, \hat{Q}_{12}, \dots\}$ could be consistent with an icosahedral symmetry, all buckled objects describable by the theory of elastic shells in fact lie on a universal curve parametrized by the value of YR^2/κ . Deviations from this curve would presumably describe biological features such as the protrusions of the adenovirus in Fig. 2.

In Sec. II, we describe our theoretical results for disclination buckling in the icosadeltahedral spherical shells proposed by Caspar and Klug as models of viruses [7]. The energy, mean-square asphericity, and spherical harmonic content of these shells are determined as a function of the Foppl-von Kármán number, discussed above,

$$\gamma = YR^2/\kappa. \quad (7)$$

Most viruses have either Foppl-von Kármán number $\gamma \lesssim 150$ (implying a close to spherical shape) or $200 \lesssim \gamma \lesssim 1500$ (noticeably buckled). Higher von Kármán numbers describing objects with very sharp corners cannot be obtained for viruses with $R \lesssim 0.2\mu\text{m}$ composed of finite size proteins. Of course, very high von Kármán numbers are possible for spherical vesicles with crystalline order composed of much smaller lipid molecules [19, 20].

We have studied the scaling of the curvature C at the creases formed after the shells buckle for large γ . We eventually recover the scaling proposed and studied in other geometries by Lobkovsky, Witten and collaborators [16, 17], but only for very large γ , $\gamma \geq 10^7$, appropriate for the buckled icosahedral vesicles described in Ref. [20].

In Sec. III, we discuss briefly the relevance of our work to icosahedral viruses from the library of those whose structures have been determined by diffraction methods or by cryo-electron microscopy [1, 2, 3, 9]. For viruses

large enough to buckle, the model seems to account well for the deviation from the spherical shape using the single adjustable parameter γ . These fits in turn provide information about the ratio Y/κ of the Young's modulus to the bending rigidity. We also discuss the possible relevance of spontaneous curvature terms and outward pressure induced by packaged DNA and RNA in this Section. See Ref. [24] for a discussion of similar issues for the shapes of liquid membranes with a spherical topology.

II. DEFECTS ON CURVED SURFACES

Topological defects play a very important role in crystalline matter. A particularly common type of defect, the dislocation, is largely responsible for the strength of materials, and in two-dimensional systems the unbinding of dislocations may drive the crystal into a hexatic phase [25]. Disclinations on the other hand, are much less common in the crystalline phase because of their very large energy. In quasi-two-dimensional curved surfaces, however, the situation may be quite different. The Gaussian curvature of the surface will “screen” out the strain around the defect and thus lower the energy. Moreover, when a crystalline surface is bent to form a closed surface with spherical topology, defects are necessarily introduced into the lattice. For a triangular lattice on a sphere the number of disclinations has to be at least 12. More generally, the difference $N_5 - N_7$ between the number of fivefold disclinations and the number of sevenfold disclinations (assuming defects with coordination numbers other than 5, 6 or 7 are absent) is precisely 6 times the Euler characteristic χ of the triangulated surface, i.e., $N_5 - N_7 = 6\chi = 12(1-g)$, where g is the genus or number of handles. Thus for shapes such that $g = 0$ (the sphere) and torii with extra handles ($g \geq 2$), the ground state must necessarily contain disclinations. (A simple torus has genus $g = 1$, so there is no topological necessity for defects.)

In this section we study closed surfaces of spherical topology. The 12 disclinations present in the crystalline lattice structure can be expected to dominate the energetics and affect the overall shape of the structure. The repulsive interaction between the 12 disclinations will favor an arrangement which maximizes their separation. Absent an instability toward grain boundaries [15], this leads to a configuration with icosahedral symmetry, where the disclinations sit at the vertices. We show below that, as a result of competition between strain and bending energies, these structures may undergo a buckling-like transition (smeared by finite size effects) from a smooth round shape to a sharply faceted shape as the size or elastic constants are varied.

A. Disclination Buckling on Spheres

We assume a thin shell described by a continuum elastic theory, with energy $\mathcal{H} = \mathcal{H}_s + \mathcal{H}_b$ [5], including both an in-plane stretching energy,

$$\mathcal{H}_s = \frac{1}{2} \int dS (2\mu u_{ij}^2 + \lambda u_{kk}^2), \quad (8)$$

where u_{ij} is the strain tensor, μ and λ are the 2D Lamé coefficients, and a bending energy,

$$\mathcal{H}_b = \frac{1}{2} \int dS (\kappa H^2 + 2\kappa_G K), \quad (9)$$

where κ is the bending rigidity, κ_G the Gaussian rigidity, H and K the mean and Gaussian curvatures, respectively. (If R_1 and R_2 are the principal radii of curvature, $H = 1/R_1 + 1/R_2$ and $K = 1/R_1 R_2$ [5].) For a closed surface with fixed topology the Gaussian curvature integrates to a constant (provided that κ_G is constant) and will henceforth be dropped, as it will have no influence on the shape. Instead of the Lamé coefficients we will use the 2D Young's modulus Y and the Poisson ratio ν , which are given by

$$Y = \frac{4\mu(\mu + \lambda)}{2\mu + \lambda}, \quad \nu = \frac{\lambda}{2\mu + \lambda}. \quad (10)$$

Taking the variation of \mathcal{H} with respect to coordinates parameterizing the surface leads to the Foppl-von Kármán equations which are highly nonlinear and whose solution even in simple geometries is very difficult [5].

The energy of disclinations on flexible crystalline membranes was studied by Seung and Nelson in Ref. [13]. As discussed in the Introduction, for a thin flat plate of finite radius R with an isolated 5-fold disclination at the center, the energy grows quadratically with the radius, $E_{\text{flat}} \simeq AYR^2$, where $A \approx \pi/288$ is a numerical constant. If the disclination is allowed to buckle out of the plane this energy is reduced, and grows logarithmically for large R with a coefficient proportional to κ . In the inextensional limit $Y \rightarrow \infty$ the problem simplifies considerably and the energy is $E_{\text{buckled}} \simeq B\kappa \ln(R/a)$, where $B \approx \pi/3$ and a the lattice constant. Thus, for small plates the flat solution is lower in energy, whereas for large plates the buckled solution wins. An instability separating these two regimes occurs when $E_{\text{flat}} \approx E_{\text{buckled}}$, or $YR^2/\kappa \approx B/A$. A detailed calculation in Ref. [13] found the transition at a critical value of $YR^2/\kappa \approx 154$.

The spherical shapes of icosahedral symmetry we are interested in here can approximately be thought of as being composed of 12 disclinations, and should therefore undergo a similar transition from flat to buckled. Because the surface of the sphere is already curved, and hence breaks the up-down symmetry that was present for a thin plate, it is not clear that a sharp instability survives in this case. However, even if this is the case, we might still expect to see remnants of the transition in the form of a sharp if not singular crossover. We construct

below simple estimates of the energies and transitions involved.

The total energy of the closed shell in the vicinity of the transition is approximately 12 times the energy of a disclination (with radius approximately equal to the radius of the sphere), plus contributions from the background curvature of a sphere, given approximately by $8\pi\kappa + 4\pi\kappa_G$. In the inextensional limit the short distance cutoff in the buckled disclination energy was provided by the lattice constant. For finite Y the cutoff is determined instead by a balance of strain and bending. We may in this case approximate the buckled disclination by a flat inner region $r < R_b$ with energy AYR_b^2 and an outer buckled region $r > R_b$ with energy $B\kappa \ln(R/R_b)$. Minimizing the sum with respect to R_b gives $YR_b^2/\kappa = B/2A$, and $E \simeq \kappa B \left(\frac{1}{2} + \ln(R/R_b) \right)$.

Because the disclination energy is independent of the two-dimensional Poisson ratio and the Gaussian rigidity drops out, the solution depends only on a single dimensionless parameter, $\gamma = YR^2/\kappa$, which we term the Foppl-von Kármán number. Note that, if the 2D elastic theory derives from a thin shell of finite thickness d built from a 3D isotropic elastic medium, we have $\gamma = 12(1 - \nu_3^2)(R/d)^2$, where ν_3 is the three-dimensional Poisson ratio, a result independent of the 3D Young's modulus Y_3 [5]. In summary, we then expect the energy of the closed shell with twelve disclinations to approximately be

$$\frac{E}{\kappa} \simeq \begin{cases} 6B\gamma/\gamma_b + D, & \gamma < \gamma_b \\ 6B(1 + \ln(\gamma/\gamma_b)) + D, & \gamma > \gamma_b \end{cases}, \quad (11)$$

where $\gamma_b = YR_b^2/\kappa$. The background curvature gives a constant contribution $D \approx 4\pi(2 + \kappa_G/\kappa)$, leading as well to a small shift in the disclination energies and hence in A and B . For a perfect sphere, e.g., $12A \approx 0.604\pi/36$ [15].

As the disclinations become more sharply buckled the whole structure will become more faceted. This leads to the formation of ridges connecting the vertices of the icosahedron. The energy of similar ridges has been studied recently [16, 17], uncovering some remarkable scaling relations. As the ridges become sharper upon increasing γ , the energy will increase as $E_{\text{ridge}}/\kappa \simeq 1.24\alpha^{7/3}(YL^2/\kappa)^{1/6}$, where α is the angle in radians and L is the length of the ridge. In this regime the shape is very close to an icosahedron with sharp facets, with $\alpha \approx 0.365$ and $L \approx 1.23R$, and a total of 30 ridges. In the limit of very large $\gamma = YR^2/\kappa$ the energy should therefore crossover to

$$E/\kappa \simeq C\gamma^{1/6} + \text{const.}, \quad \gamma \rightarrow \infty, \quad (12)$$

where $C \approx 3.8$.

To check these arguments and to calculate more properties of the shells we now present numerical calculations.

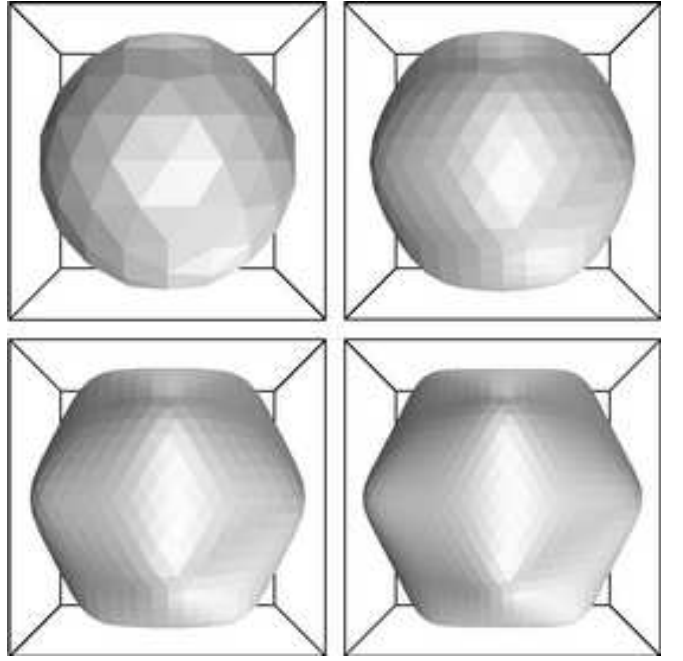


FIG. 5: Numerically calculated shapes with (h, k) indices $(2,2)$, $(4,4)$, $(6,6)$, and $(8,8)$ for fixed $\tilde{\kappa} = 0.25$, and fixed spring constant $\epsilon = 1$. The Foppl-von Kármán numbers for these shapes are $\gamma \approx 45, 176, 393$ and 694 .

B. Numerical Results

For numerical calculations it is useful to consider discretized versions of Eqs. (8) and (9) [13]:

$$\mathcal{H}_s = \frac{\epsilon}{2} \sum_{\langle ij \rangle} (|\mathbf{r}_i - \mathbf{r}_j| - a)^2 \quad (13)$$

and

$$\mathcal{H}_b = \frac{\tilde{\kappa}}{2} \sum_{\langle IJ \rangle} (\hat{\mathbf{n}}_I - \hat{\mathbf{n}}_J)^2. \quad (14)$$

Here $\langle ij \rangle$ denote pairs of nearest neighbor vertices (which we identify with the centers of the capsomers of a virus), with positions \mathbf{r}_i , and $\langle IJ \rangle$ pairs of nearest neighbor plaquettes of a triangulated surface, with unit normals $\hat{\mathbf{n}}_I$. In the continuum limit this model becomes equivalent to Eqs. (8) and (9) with parameters [13]

$$Y = \frac{2}{\sqrt{3}}\epsilon, \quad \nu = \frac{1}{3} \quad (15)$$

$$\kappa = \frac{\sqrt{3}}{2}\tilde{\kappa}, \quad \kappa_G = -\frac{4}{3}\kappa \quad (16)$$

The relation $\kappa_G = -4\kappa/3$ was calculated by comparing the bending energy of a triangulated cylinder and sphere with the corresponding continuum expressions, and differs from the one used in Ref. [13]. Closed triangular surfaces of icosahedral symmetry are constructed for non-negative integers (h, k) according to the geometric principles of Caspar and Klug [7], and the minimum energy

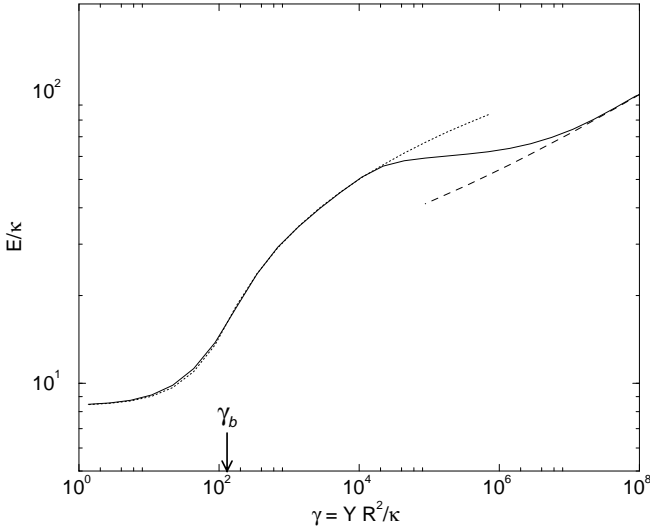


FIG. 6: Total energy. Dotted and dashed lines are fits to Eq. (11) and (12), respectively. The arrow indicates the value of γ_b obtained from the fit.

configuration is found numerically using a conjugate gradient method for different values of $\tilde{\kappa}$. As discussed in the Introduction, the integers (h, k) denote the number of steps along the two lattice vectors between two neighboring disclinations of the structure. Figure 5 shows some examples of the resulting shapes. Shapes of varying size with “T-numbers” as large as $T = h^2 + hk + k^2 \approx 1500$ are studied. Below we calculate some properties of the shells to characterize the shapes quantitatively.

1. Energy

We first plot the total energy as a function of the Foppl-von Kármán number γ in Fig. 6. Similar to results for an isolated disclination in a disk with free boundary conditions [13], the energy crosses over from a “flat” regime dominated by stretching energy to a “buckled” regime dominated by bending energies. Fitting the functional form Eq. (11) gives $A \approx 0.005$, $B \approx 1.30$, $\gamma_b \approx 130$, which compares quite well with the estimates above. For large $\gamma \gtrsim 10^7$ a crossover to the form given by Eq. (12) (indicated by the dashed line in the figure) occurs.

2. Asphericity

As a measure of the deviation from a perfectly spherical shape centered on the origin we calculate the mean squared asphericity, defined by

$$\frac{\langle \Delta R^2 \rangle}{\langle R \rangle^2} = \frac{1}{N} \sum_{i=1}^N \frac{(R_i - \langle R \rangle)^2}{\langle R \rangle^2}, \quad (17)$$

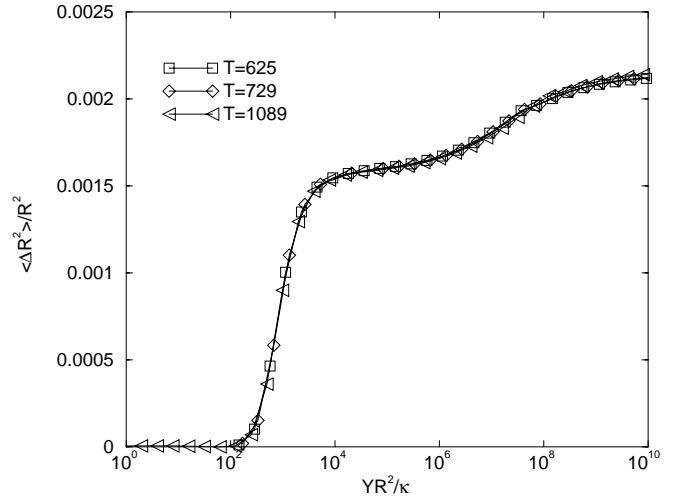


FIG. 7: Mean squared asphericity (see Eq. (17)) as a function of $\gamma = YR^2/\kappa$ for various “triangulation numbers” $T = h^2 + hk + k^2$. Data from shapes of three different sizes collapse onto a single universal curve, indicating that the continuum limit has been reached for these sizes.

where R_i is the radial distance of vertex i and $\langle R \rangle$ is the mean radius,

$$\langle R \rangle = \frac{1}{N} \sum_{i=1}^N R_i. \quad (18)$$

The result, which is displayed in Fig. 7, shows a rather sharp, but non-singular crossover from spherical shape to faceted at roughly $\gamma = YR^2/\kappa \approx 150$. The second increase around $YR^2/\kappa \approx 10^7$ coincides roughly with the sharpening of the ridges, where the asymptotic scaling in Eq. (12) sets in. Note that the log-linear plot of Fig. 7 extends the range of γ in Fig. 4 by six orders of magnitude.

3. Icosahedral spherical harmonics

We first expand the radial density of points on the surface in spherical harmonics,

$$R(\theta, \phi) = \sum_{l,m} Q_{lm} Y_{lm}(\theta, \phi), \quad (19)$$

where the density $R(\theta, \phi)$ is defined by

$$R(\theta, \phi) = \sum_j R_j \delta(\phi - \phi_j) \delta(\cos \theta - \cos \theta_j), \quad (20)$$

and (R_j, θ_j, ϕ_j) represents the polar coordinates of vertex j . From the coefficients Q_{lm} , we form the rotation-invariant combinations

$$Q_l^2 = \frac{4\pi}{2l+1} \sum_{m=-l}^l |Q_{lm}|^2. \quad (21)$$

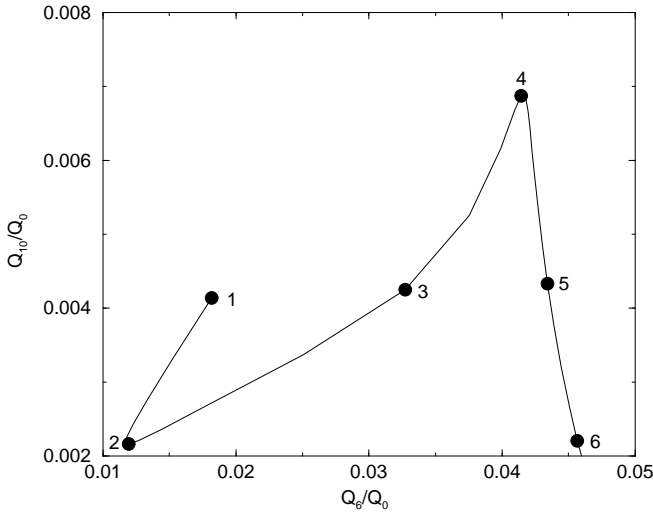


FIG. 8: Combination of spherical harmonics (see text), which fall on a universal curve for large enough shells. Points for triangulations defined by $(h, 0), h = 5, 6, \dots, 25$ were used to construct the solid curve. For $h < 5$ deviations due to discreteness become large and those points have been omitted for clarity. Points labeled 1–6 correspond to $\gamma \approx 0.5, 30, 1000, 15000, 8 \times 10^6$ and 2.5×10^8 , respectively.

For a shape of icosahedral symmetry the Q_l 's are non-zero only for $l = 0, 6, 10, \dots$ [23]. We plot, in Fig. 8, Q_{10}/Q_0 vs Q_6/Q_0 , which for large shells should fall on a universal curve parameterized by YR^2/κ . Note that *any* point in the $(Q_6/Q_0, Q_{10}/Q_0)$ -plane would be consistent with an icosahedral symmetry. Continuum elastic theory, however, predicts a *universal* set of functions $Q_l(\gamma)$ parametrized only by the Foppl-von Kármán number. The buckling transition occurs between the points labeled 2–4 in Fig. 8, while the crossover to the ridge scaling for very large γ happens between points 4–6.

4. Curvature

The curvature C across the midpoints of the ridges connecting the vertices of the icosahedra is plotted in Fig. 9. As $\gamma = YR^2/\kappa$ increases through the transition the ridges get sharper and the shape becomes more faceted. A perfect sphere would have $C = 1/R$. However, as seen in Fig. 9, CR saturates to a slightly smaller value, $\simeq 0.7$, for very small γ , implying that the shape is not perfectly spherical below the buckling transition. In fact, there is a weak tendency toward a dodecahedral shape (which is the dual to the icosahedron). The effect is hardly visible (cf. Fig. 7), however. The data for large shells is well described by a scaling form

$$C = R^{-1} F(YR^2/\kappa), \quad (22)$$

depending on the single parameter γ . In the limit of large arguments $\gamma \rightarrow \infty$, we find $F(\gamma) \rightarrow \gamma^{1/6}$, consistent with

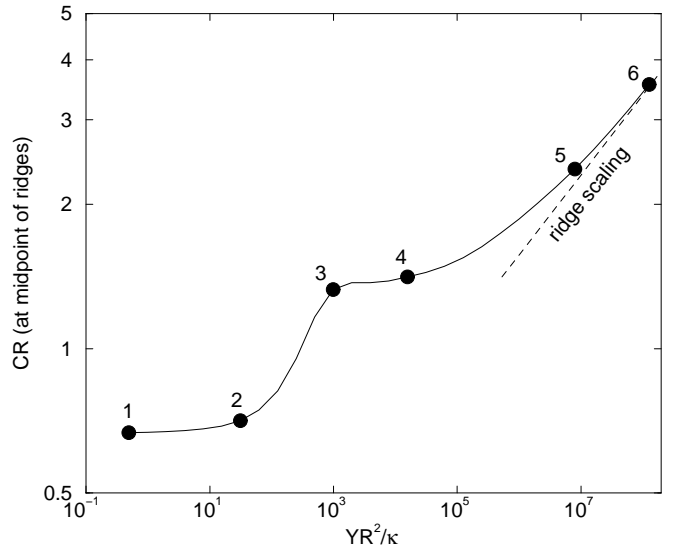


FIG. 9: Curvature at the midpoints of the ridges. The points labeled 1–6 are for the same values of γ as in Fig. 8. The dashed line shows the asymptotic scaling behavior $\sim \gamma^{1/6}$.

the scaling arguments of Lobkovsky *et al.* [16, 17]. Note, however, that γ 's well in excess of 10^6 are required before one begins to see this asymptotic result of “ridge scaling”.

III. DISCUSSION

We have analyzed a model, based on the (highly non-linear) physics of thin elastic shells, which may be suitable for describing the shapes of large viruses and of large vesicles with crystalline order in the lipids. Application of our results to vesicles [19, 20] seems straightforward, once sufficiently precise freeze fracture or confocal microscope images become available. Figure 10 illustrates two highly faceted shapes we found for the large Foppl-von Kármán numbers or “vK's” which might be relevant to the experiments of Ref. [20]. One complication neglected here concerns possible phase separation of the binary lipid mixtures studied by Dubois *et al.* in the vicinity of the 12 disclinations [20]. It would be interesting to investigate this effect, although a modest enrichment of one lipid species near a disclination could be incorporated into a renormalized core energy. As discussed in Sec. II B, vK's in excess of 10^6 are required to see clearly the interesting scaling predictions of Refs. [16] and [17]. In the remainder of this section, we comment on the relevance of our work to spherical viruses [1, 3, 7, 9], where the vK's are of order a few thousand or less.

Ref. [3] compiles cryo-electron micrographs and other data on approximately thirty different viruses, arranged in order of increasing size. These images highlight the trend that small viruses are round and larger viruses are more faceted. We view faceted viruses as the result of 12 simultaneous buckling transitions, centered on

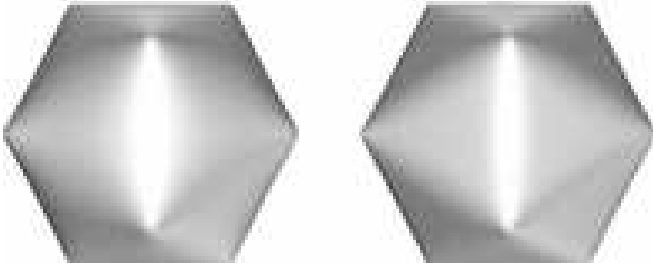


FIG. 10: Two shapes for the large Foppl-von Kármán numbers $\gamma = 15600$ and 8×10^6 (points 4 and 5 in Fig. 8–9), illustrating the sharpening of the ridges in the ridge scaling regime.

12 disclinations, similar to the buckling of an *isolated* disclination centered on a disk with open boundary conditions [13]. The *spherical* packing of the protein capsomers in viruses not only forces in twelve disclinations (which we assume reside at the vertices of an icosahedron) [7], but also breaks the up/down symmetry of a disk with respect to the direction of buckling. Hence, we expect (and find numerically) that the sharp buckling transition with increasing size in Ref. [13] is smeared out. As shown in Fig. 11 for bacteriophage HK97 (with 72 capsomers), good one parameter fits in real space to the full three dimensional shape of spherical viruses are possible. Our best fit for Foppl-von Kármán number of this mature form of HK97 is $\gamma = YR^2/\kappa = 1480$, from which we can extract the ratio of the Young's modulus Y to the bending rigidity κ , given that the virus diameter is $2R = 55\text{nm}$ [3]. The *precursor* capsid or “prohead” of HK97 is rather spherical, in contrast to the larger, more faceted mature infectious virus shown in Fig. 11 [27]. It seems likely that this virus particle undergoes a buckling transition as it passes from the prohead to its mature infectious form. Indeed, the prohead shell is wrinkled or corrugated relative to the mature form [27]. It seems reasonable to regard this transformation as a change in the effective thickness d of the viral shell: d' of the prohead goes to $d < d'$ in the mature form. As discussed in Sec. II A, $\gamma = 12(1 - \nu_3^2)(R/d)^2$ if we approximate the shell by a uniform isotropic elastic medium with Poisson ratio ν_3 [5]. Since R increases from $47\text{nm} \rightarrow 55\text{nm}$ as d decreases, it is plausible that $\gamma \sim (R/d)^2$ rises and that the transformation from prohead \rightarrow head is accompanied by a buckling transition.

Figure 12 shows a similar fit to the yeast virus, which yields $\gamma = YR^2/\kappa = 547$. The diameter of the yeast virus is $2R = 43\text{nm}$, which leads to the conclusion that $[Y/\kappa]_{\text{yeast}} = 0.30\text{nm}^{-2}$. Note that $[Y/\kappa]_{\text{HK97}} = 0.49\text{nm}^{-2}$, consistent with the arguments given in the Introduction that spherical viruses have roughly similar elastic constants.

Our models for virus shells are based on two important assumptions. The first is the neglect of a spontaneous curvature term [26] in bending energies such as Eq. 9. Such a term might be significant if the viral build-

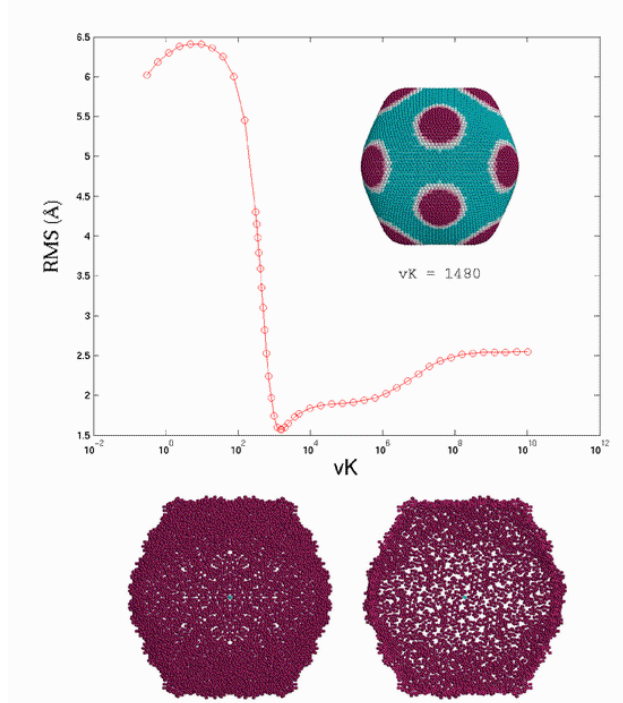


FIG. 11: Real space fit to a virus structure. The curve shows the root-mean-square deviation from the experimental virus shell of bacteriophage HK97 (full virus and cross section shown in the lower part of the figure) and the theoretically calculated shape. The best fit occurs at the minimum for $\gamma \approx 1480$ and the corresponding shape is depicted in the inset. Shading indicates the distance of the shell from the center.

ing blocks had a pronounced conical shape similar to, say, surfactant molecules in a micelle [26, 28] or laboratory cork stoppers. Several lines of evidence suggest that neglect of this term might be justified. Although certain virus scaffolding proteins (which can act as templates for early phases of construction) do have a conical shape, these are discarded in the mature icosahedral viruses of interest to us here [1]. It is hard to see a strong mechanism for precisely-defined hinge angles in very large viruses composed of many capsomers [29, 30]. In vitro assembly experiments on the polyoma virus do produce spherical aggregates with 12, 24 and 72 pentameric units depending on conditions of pH, calcium concentration, etc [31], which could be accounted for by a spontaneous curvature term. Although we neglect spontaneous curvature here, it is certainly possible that the physics of small viruses (or the scaffolding proteins themselves) are influenced by such an energy, as has been explored by Bruinsma, Rudnick and Gelbart [32].

In general our work is more likely to be applicable to *large* viruses, for which simple continuum models can be justified. Icosahedral viruses are usually composed of a combination of 5- and 6-fold symmetric packing units, with the twelve 5-fold units centered on the vertices of an icosahedron (the polyoma virus SV40 [3] with its 72

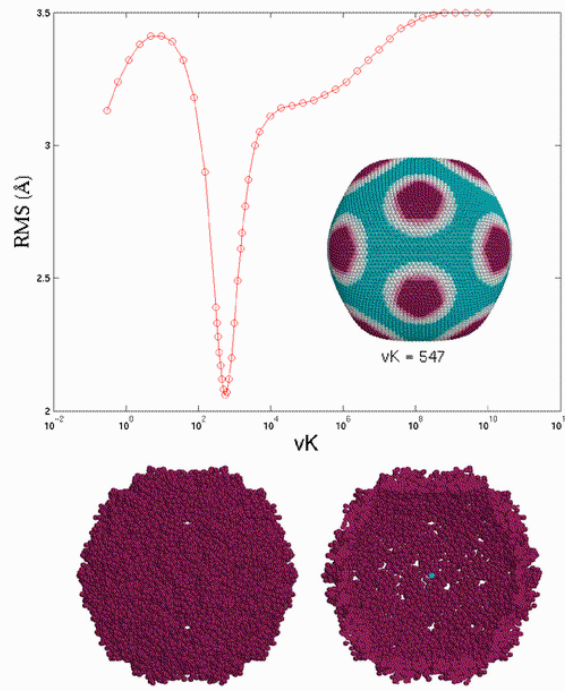


FIG. 12: Real space fit to Yeast virus L-A with inset and actual virus as described in Fig. 11. The best fit occurs for $\gamma = 547$.

identical pentamers is an exception). Because the strain energies which lead to buckling extend far from the disclinations which produce them [13], we would expect our results for large viruses to be insensitive to differences

in the shapes of packing elements. Special packing elements at the twelve 5-fold sites could be incorporated into a disclination core energy.

A second key assumption is our neglect of the osmotic pressure due to the confined DNA or RNA package of the virus [4]. Here we can appeal to an experiment. Earnshaw and Harrison [33] have compared the structure of phage lambda (P22) with its full complement of DNA to the structure of lambda mutants containing only 78% of the native DNA. Although changes in the details of DNA packing can be detected, the protein shell itself is unchanged. Thus, due either to DNA condensation or an exceptionally strong shell, the osmotic pressure of the DNA is insufficient to change the shape. Of course, the nucleic acid content of a virus could nevertheless play an important role in shell assembly [34].

Acknowledgments

It is a pleasure to acknowledge valuable advice and conversations with S. Harrison, B. Shraiman, J. Johnson, S. Burley, R. Bruinsma, P. Lenz and T. Zemb. Work by drn and jl was supported in part by the National Science Foundation, through grant DMR-0231631 and through the Harvard Material Science and Engineering Center through grant DMR-0213805. drn would like to acknowledge the hospitality and support of the Center for Studies in Physics and Biology at Rockefeller University in the fall of 2000, where this work was begun. jl acknowledges support from the Swedish Research Council (VR). lm is an Alfred P. Sloan Research Fellow, and also acknowledges support of John F. and Virginia B. Taplin Award.

[1] Structural Biology of Viruses, edited by W. Chiu, R. M. Burnett and R. L. Garcea (Oxford University Press, New York 1997).

[2] S. C. Harrison, “What do Viruses Look Like?”, Harvey Lectures 85, 127 (1991).

[3] T. S. Baker, N. H. Olson and S. D. Fuller, “Adding the Third Dimension to Virus Life Cycles”, Microbiology and Molecular Biology Reviews, 63, 862 (1999).

[4] D. E. Smith, S. J. Tans, S. B. Smith, S. Grimes, D. L. Anderson and C. Bustamante, “The bacteriophage ϕ 29 portal motor can package DNA against a large internal force”, Nature 413, 748 (2001).

[5] L.D. Landau and I.M. Lifshitz, *Theory of Elasticity* (Pergamon, New York, 1975).

[6] F. Crick and J. D. Watson, “The Structure of Small Viruses”, Nature 177, 473 (1956).

[7] D. Caspar and A. Klug, “Physical Principles in the Construction of Regular Viruses”, Cold Spring Harbor Symposium on Quantitative Biology, 27, 1 (1962).

[8] H.M.S. Coxeter, *Introduction to Geometry* (Wiley and Sons, Inc., New York 1969), Chaps. 19–21.

[9] V. Reddy, P. Natarajan, B. Okerberg, K. Li, K. Damodaran, M. R. Brooks III, J. Johnson, “Virus Particles Explorer (VIPER), a Website for Virus Capsid Structures and Their Computational Analyses”, Journal of Virology 75, 11943 (2001); P. L. Stewart, R. M. Burnett and S. D. Fuller, “Image reconstruction reveals the complex molecular organization of adenovirus”, Cell 67, 145-167 (1991).

[10] A. G. Murzin, S. E. Brenner, T. Hubbard, C. Chothia, “SCOP: a structural classification of proteins database for the investigation of sequences and structures”, J. Mol. Biol. 247, 536-540 (1995), <http://scop.mrc-lmb.cam.ac.uk/scop/data/scop.b.c.bd.b.html>.

[11] M. Carrion-Vazquez, A. F. Oberhauser, T. E. Fisher, P. E. Marszalek, H. Li, J. M. Fernandez, “Mechanical design of proteins studied by single-molecule force spectroscopy and protein engineering”, Prog. Biophys. Mol. Biol. 74, 63-91 (2000).

[12] M. S. Kellermayer, C. Bustamante, H. L. Granzier, “Mechanics and structure of titin oligomers explored with atomic force microscopy”, Biochim. Biophys. Acta. 1604, 105-14 (2003).

[13] S. Seung and D. R. Nelson, “Defects in Flexible Membranes with Crystalline Order”, Phys. Rev. A 38, 1005 (1988).

[14] D. R. Nelson and L. Peliti, "Fluctuations in Membranes with Crystalline and Hexatic Order", *Journal de Physique* **48**, 1085 (1987), and references therein.

[15] M.J. Bowick, D.R. Nelson, and A. Travesset, "Interacting Topological Defects in Frozen Topographics," *Phys. Rev. B* **62**, 8738 (2000); (arXiv:cond-mat/9911379); See also A. R. Bausch, M. J. Bowick, A. Cacciuto, A. D. Dinsmore, M. F. Hsu, D. R. Nelson, M. G. Nikolaides, A. Travesset, and D. A. Weitz, "Grain Boundary Scars and Spherical Crystallography", *Science* **299**, 1716 (2003).

[16] A. E. Lobkovsky, "Boundary layer analysis of the ridge singularity in a thin plate", *Phys. Rev. E* **53**, 3750 (1996).

[17] A. E. Lobkovsky and T. A. Witten, "Properties of Ridges in Elastic Membranes", *Phys. Rev. E* **55**, 1577 (1997).

[18] E. Cerdà and L. Mahadevan "Conical Surfaces and Crescent Singularities in Crumpled Sheets", *Phys. Rev. Lett.* **80**, 2358 (1998).

[19] A. E. Blaurock and R. C. Gamble, "Small Lecithin Vesicles Appear to be Faceted below the Thermal Phase Transition", *J. Membrane Biol.* **50**, 187 (1979); E. Sackmann and R. Lipowsky, "Handbook of Biological Physics", Vol. 1B, ed. A. J. Hoff, (North-Holland, Amsterdam, 1995).

[20] M. Dubois, B. Demé, T. Gulik-Krzywicki, J.-C. Dedieu, C. Vantrin, S. Desert, E. Perz, and T. Zemb, "Self-Assembly of Regular Hollow Icosahedra in Salt-free Catanionic Solutions.", *Nature* **411**, 672 (2001).

[21] Y. Kantor and D. R. Nelson, "Phase Transitions in Flexible Polymeric Surfaces", *Phys. Rev. A* **36**, 4020 (1987).

[22] X. Yan, N. H. Olson, J. L. Van Etten, M. Bergoin, M. G. Rossmann, and T. S. Baker, "Structure and Assembly of Large Lipid-Containing dsDNA Viruses", *Nature Structural Biology* **7**, 101 (2000).

[23] P. Steinhardt, D. R. Nelson and M. Ronchetti, "Bond orientational order in liquids and glasses", *Phys. Rev. B* **28**, 784 (1983).

[24] For an analogous exploration of the shapes of liquid membranes with a spherical topology, see U. Seifert, "Configurations of Fluid Membranes and Vesicles", *Advances in Physics* **46**, 13 (1997); See also H. Noguchi, "Polyhedral vesicles: A Brownian dynamics simulation", *Phys. Rev. E* **67**, 041901 (2003).

[25] See, e.g., D.R. Nelson, *Defects and Geometry in Condensed Matter Physics* [Cambridge University Press, Cambridge, 2002].

[26] See, e.g., S. Leibler in "Statistical Mechanics of Membranes and Interfaces", edited by D. R. Nelson, T. Piran and S. Weinberg (World Scientific, Singapore 1989).

[27] J. F. Conway, W. R. Wikoff, N. Cheng, R. L. Duda, R. W. Hendrix, J. E. Johnson, and A. C. Steven, "Virus Maturation Involving Large Subunit Rotations and Local Refolding", *Science* **292**, 744 (2001).

[28] S. A. Safran, "Statistical Thermodynamics of Surfaces, Interfaces and Membranes", (Addison-Wesley, New York 1994).

[29] V. S. Reddy, H. A. Giesing, R. T. Morton, A. Kumar, C. B. Post, C. L. Brooks III, and J. E. Johnson, "Energetics of quasiequivalence: computational analysis of protein-protein interactions in icosahedral viruses", *Biophys.* **74**, 546 (1998).

[30] P. K. Sorger, P. G. Stockley, S. C. Harrison, "Structure and Assembly of Turnip Crinkle Virus .2. Mechanism of Reassembly Invitro", *J. Mol. Biol.* **191**, 639 (1986).

[31] D. M. Salunke, D. L. Caspar, and R. L. Garcea, "Polymorphism in the assembly of polyomavirus capsid protein VP1", *Biophys.* **56**, 887 (1989).

[32] R. F. Bruinsma, J. Rudnick, W. M. Gelbart, "Viral self-assembly as a thermodynamic process", arXiv:cond-mat/0211390.

[33] W. C. Earnshaw and S. C. Harrison, "DNA arrangement in Isometric Phage Heads", *Nature* **268**, 598 (1977).

[34] J. Rudnick and R. F. Bruinsma, "Icosahedral packing of RNA viral genomes", arXiv:cond-mat/0301305, and references therein.